Applied Water Science (2021) 11:90
https://doi.org/10.1007/s13201-021-01420-6

ORIGINAL ARTICLE

Pb(II) removal in water via adsorption onto deep eutectic solvent fabricated activated carbon

Aloysius Akaangee Pam[1] · Zul Adlan Mohd Hir[2] · Abdul Halim Abdullah[3,4] · Yen Ping Tan[3]

Received: 24 September 2020 / Accepted: 4 May 2021 / Published online: 21 May 2021

Abstract

In our current work, we have established a novel approach in the synthesis of a new adsorbent by using choline chloride and urea (DES)/orthophosphoric acid (H_3PO_4) as our activating agent and palm kernel shell (PKS) as our precursor. The resulting activated carbon (DES/H_3PO_4-6002:3) was used to adsorb Pb(II) from aqueous solution. Characterization of DES-H_3PO_4-6002:3 by nitrogen adsorption/desorption isotherm measurements, scanning electron microscopy (SEM), X-ray photoelectron spectroscopy (XPS) and thermogravimetric analysis (TGA) demonstrated good micropores structure and high surface area that makes DES/H_3PO_4-600 2:3 a suitable alternative for liquid phase adsorption. The fundamental batch experiment of DES/H_3PO_4-600 2:3 was investigated by different parameters (such as concentration, pH, temperature and absorbent dose). The results obtained indicated that Langmuir model and pseudo-second-order equation best fit the data, indicating that the adsorption was controlled by chemical reaction and monolayer uptake. In addition, the fabrication of DES/H_3PO_4 AC exhibits good potential for Pb(II) ions uptake, including its high adsorption capacity (97.1 mg/g) and good recyclability. The future potential of this works lies in the identification of alternatives to environmental benign synthesis AC and reuse of Pb(II) ion–laden biosorbent after heavy metal uptake.

Keywords DES/H_3PO_4 · Pb(II) · Adsorption · Reusability · Palm kernel shell

Introduction

Presently, pollution of water ecosystem with heavy metal ions is a global problem considering the long-term risk both to the human well-being and to the environment. Due to industrialization, untreated or partially treated water is discharged into public land from sewage treatment plants containing toxic compounds, so water is polluted every day (Inamuddin and Ismail 2010). Lead, one of the major constituents in aqueous waste, is a priority pollutant (as considered by USEPA) (Pei et al. 2019) and has a legacy of being accumulative poison of ecological succession and bioconcentration (Pei et al. 2019). The allowable concentration of Lead ions in wastewater (WHO approved) is approximately 0.01 mg/L (Kumar et al. 2019). Moreover, long exposure to lead especially at acute level could shut down the biochemical pathways causing damage to the central peripheral nervous (Alghamdi et al. 2019; Penugonda et al. 2006), kidney (Boskabady et al. 2018; Wani et al. 2015), reproductive system of persons (Fenga et al. 2017), often leading to death as a sequelae of lead poisoning. The release of Pb into water ecosystem is often due to discharge related to certain

✉ Aloysius Akaangee Pam
aloysius.pam@fulokoja.edu.ng

Zul Adlan Mohd Hir
zuladlan@uitm.edu.my

Abdul Halim Abdullah
halim@upm.edu.my

Yen Ping Tan
typ@upm.edu.my

1 Chemistry Department, Faculty of Science, Federal University Lokoja, Lokoja P.M.B. 1154, Nigeria

2 Faculty of Applied Sciences, Universiti Teknologi MARA Pahang, 26400 Bandar Tun Abdul Razak Jengka, Pahang, Malaysia

3 Chemistry Department, Faculty of Science, Universiti Putra Malaysia, 43400 Serdang, Selangor, Malaysia

4 Material Synthesis and Characterization Laboratory, Institute of Advanced Technology, Universiti Putra Malaysia, 43400 Serdang, Selangor, Malaysia

industrial units, including battery manufacturing (Alghamdi et al. 2019; Jan et al. 2015), mining (C. P. Wang et al. 2011a, b), smelting (Edokpayi et al. 2015), oil refining (Alghamdi et al. 2019) and so on located in close proximity to the water bodies. In addition to industries, another concerned is corrosion of plumbing materials (water pipes) (Boskabady et al. 2018) and lead applications in agriculture (in fertilizers and pesticides) and in leaded gasoline (Jan et al. 2015). Application of conventional methods (electrochemical treatment, precipitation, reduction, membrane separation and so on) in the treatment of water with metal ions has some drawbacks (secondary pollution, high cost of operation and low efficiency), and adsorption onto suspended particle has shown to be cost-effective and efficient method (Fiyadh et al. 2019; He et al. 2019). Different adsorbents, including clay (Yin et al. 2018), carbon nanotubes (Dai et al. 2018), nano-TiO_2/cellulose composites (Zhang et al. 2016) and activated carbon (Kyzas and Mitropoulos 2018), are well exploited in Pb ions removal in water. Activated carbon, among various adsorbent, is a well-developed porous material with an excellent performance, and immense process applications (Ahmed et al. 2019) are widely utilized alone or alongside other materials for the treatment of lead in water (Kumar et al. 2019). Activated carbons prepared from activating reagents including KOH, $ZnCl_2$ and NaOH are usually not compatible with food industries and have high tendency for secondary pollution. To solve this problem of environmental and health concern, deep eutectic solvents (DESs)/H_3PO4 activated carbon was fabricated. Deep eutectic solvents (DES) are solvents with almost no toxicity, high recyclability, low inflammability and volatility, and total biodegradables are promising sustainable alternatives to ionic liquids and conventional solvents (Di Gioia et al. 2018). In addition to the environmentally friendly properties of DES, they are also easy to prepare (Kumari et al. 2018). These fascinating physical properties and the freedom to design DES play a vital role in many field applications, including separation, preparation of inorganic and organic materials, extraction, biotransformation, nanomaterial, electrochemistry (Kumari et al. 2018) and interactions with other compounds by surface modification, thus providing a suitable podium for functionalization, synthesis and development of adsorbents with green chemistry framework. The potential applications of DES in water treatment can be seen in functionalization of carbon nanotubes, graphene and graphene oxide, and carbon monoliths (Carriazo et al. 2012; Huang et al. 2015; Lawal et al. 2019; Wang et al. 2017) and in the synthesis of composite materials (Chen et al. 2017; Patiño et al. 2012; Tang and Row 2019).

Palm kernel shell (PKS) is an unavoidable by-product of palm oil milling industry and is disposed of by burning or dumping into open environment, which wastes as valued resources and equally causes environmental pollution. Converting PKS to activated carbon is the right direction as it will not only solve the disposal problems associated with PKS, but also serve as renewable alternative precursor for the traditional fossil fuels for preparation of activated carbon. Taking into cognizance the need for a renewable and benign adsorbent for water treatment, we exploited the unique properties of chlorine chloride (DES)/orthophosphoric acid (H_3PO_4) as new and clean approach for the preparation of activated carbon using PKS as a precursor. H_3PO_4 is well known for its eco-friendly and non-polluting nature (Sivachidambaram et al. 2017).

The study aims at converting PKS to activated carbon using DES/H_3PO_4. Additionally, promising characteristics of DES/H_3PO_4 activated carbon as a lead adsorbent was evaluated via sequences of parameters (i.e., initial pH, dosage, initial concentration and temperature) in relation to lead separation mechanism in water. The findings, which are the first study on the application of DES/H_3PO_4 in the synthesis of AC, will help to produce environmental benign AC with promising removal capacity for heavy metals in practical industrial application and promote the use of renewable alternative precursors.

Materials and methods

Materials

Lead(II) salt ($Pb(NO_3)_2$), hydrochloric acid (HCl), sodium hydroxide(NaOH), all of analytical grade were supplied by Fisher Scientific, Pittsburg, PA, USA. Chlorine chloride (ChCl), and urea ≥ 98% as revealed by the supplier (Sigma-Aldrich, St. Louis, Mo, USA), and orthophosphoric acid (concentrated H_3PO_4, Merch, Germany). Synthetic wastewater (containing Pb) was obtained by dissolving stoichiometric amount of the Pb salt in ultrapure H_2O to obtain a stock solution (1000 mg/L), and successive dilutions were made for working solution in subsequent batch experiments.

Preparation of deep eutectic solvent

To synthesis the DES, we used the method reported by Yadav and Pandey (2014). In a typical experiment, urea and choline chloride were mixed in mole ratio 2:1. To afford clear and homogeneous solution, the mixture was further stirred under heat at 80 °C. The deep eutectic solvent was then used in the preparation of activated carbon. The synthesis of the DES may be represented schematically as shown in Fig. 1a

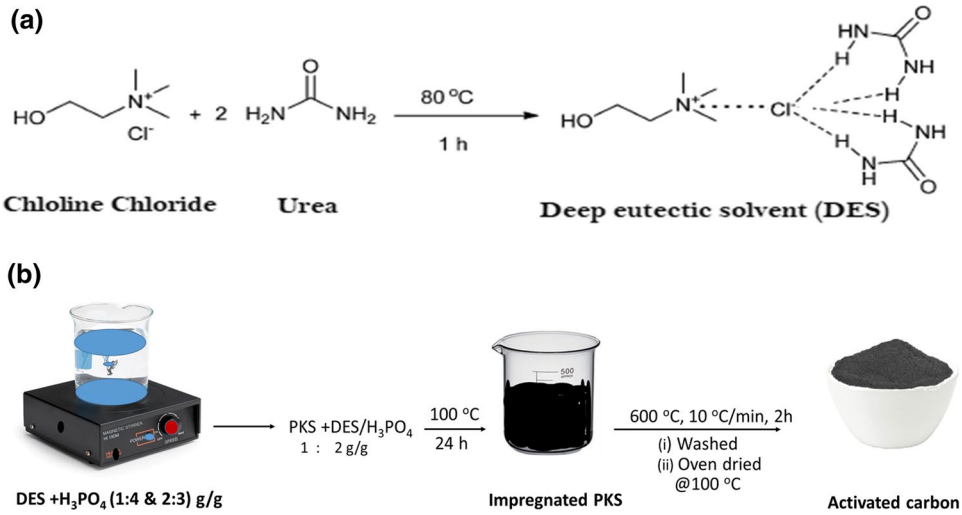

Fig. 1 Synthesis rout of DES/H_3PO_4 based adsorbent

Activated carbon preparation

To prepare the activated carbon, the experiments were conducted in three basic steps, i.e., pretreatment, impregnation and activation as depicted in Fig. 1b. The dirt particles associated with the surfaces of the PKS were removed by washing with distilled water. The washed PKS was tried under sun for about 3 days, and then, the particles size of the PKS was reduced by crushing. The activating agent (DES/H_3PO_4) was obtained by mixing choline chloride/urea (DES) and H_3PO_4 by mass (2:3 and 1:4) and for period of 3 h stirred at 25 °C. DES/H_3PO_4: PKS ratio stood fixed at 2:1. The impregnated samples were introduced into a tubular furnace and carbonized to a temperature of 500 and 600 °C differently, at a constant heating rate of approximately 10 °C/min under continuous nitrogen flow. The holding time of the various carbonization temperatures was 2 h. After the reaction time elapsed, the samples were removed from the furnace and allowed to cool under room temperature, then washed with hot distilled water severally to remove the residual acid and then dried in an oven at 100 °C to a constant weight. The resulting activated carbons were ground and collected in sample bottles for further characterization and adsorption test. A preliminary adsorption test showed that AC samples prepared at impregnation ratio of 2:3(DES:H_3PO_4) and temperature of 600 °C donated as DES/H_3PO_4-600 2:3, demonstrated better capacity for the adsorption of Pb in aqueous solution than that of DES/H_3PO_4-500 2:3, DES/H_3PO_4-500 1:4 and DES/H_3PO_4-600 1:4 (data not reported). As a result, DES/H_3PO_4-600 2:3 was characterized and used as selective adsorbent in the removal of lead in this present work. To calculate, AC yield, Eq. 1 was applied.

$$\text{Yield}(\%) = \frac{\text{Mass of sample after activation}(g)}{\text{Initial mass of dried sample}(g)} \quad (1)$$

Adsorbent characterization

Morphology of the DES/H_3PO4-600 was observed on a FESEM (FEI Nova 320). To investigate the apparent surface area and porosity of the adsorbent, absorption isotherm of nitrogen was measured at 77 K in a surface analyzer (Nova 1200, Quantachrome), via the Barrett–Joyner–Halenda and Brunauer–Emmett–Teller methods, respectively. Surface functional groups on DES/H_3PO_4-600:3 were characterized using Perkin-Elmer spectrum 100 using attenuated total reflectance techniques. The surface chemistry of DES/H_3PO_4-600 2:3 was further analyzed using XPS Kratos Axis UltraDLD with ejected photoelectron having a monochromated beam Al Kα X-ray energy source (1486.7 eV). The resulting spectra were referenced by the C1 (graphitic carbon) peak occurring at 284.6 eV (Palomo et al. 2019) using the software package (XPSPEAK41). TGA was conducted using thermogravimetric analyzer (STA600 Perkin-Elmer) over a temperature range of 0–900 °C under nitrogen flow at heating rate of 10 °C/min.

Batch adsorption experiments

To appraise the practical application of DES / H_3PO_4-600 2:3 in Pb adsorption batch experiments were tested. Achieving this goal, we conducted series of batch adsorption experiments by varying the process factors. For the dosage optimization test, we varied the adsorbent masses from 0.1 to 0.3 g. For effect of Pb initial concentration, individual metal solution of 75 to 125 mg/L of Pb was used at fixed adsorbent mass. 0.1 M either of HCl or NaOH was used to examine effect of solution pH by adjusting the metal solutions pH to the anticipated values by a pH meter, while effect of temperature was investigated between 30 and

50 °C. All experiments were done in duplicate at fixed agitation speed of 150 rpm and metal solution of 200 mL. The residue Pb in the filtrate from the suspension was analyzed using atomic adsorption spectrophotometer (thermo Scientific-s series). The amount removal (qt) and uptake rate (%) of the AC were computed according to equations in (2) and (3), respectively:

$$Q_t = \left(C_o - C_e\right) V/M \tag{2}$$

$$\text{Removal } (\%) = \left(C_o - C_e\right)/C_o \times 100 \tag{3}$$

where C_o (mg/L), C_e (mg/L), V (L) and M (g) stand for initial concentration, equilibrium concentration, volume of sample and weight of EDS/H_3PO_4-600 2:3.

Results and discussion

Characterization

Figure 2a shows the nitrogen adsorption–desorption isotherm of DES/H_3PO_4 600:3. The isotherm belongs to type 1 according to IUPAC classification, a typical characteristic of a microporous adsorbent. This result is supported by the PSD illustrated in Fig. 2b. Accordingly, the PSD appeared between 6.0 Å and 16.0 Å with a value of 11.0 Å (average pore diameter) and a total pore volume of 0.6181 cm^3/g, an indication of a microporous adsorbent. The apparent surface area estimated by BET method was 1413 m^3/g. Similarly, Su and Wang (2007); Foo and Hameed (2012); Nowicki et al. (2016) reported specific surface areas of 1423 m^2/g,

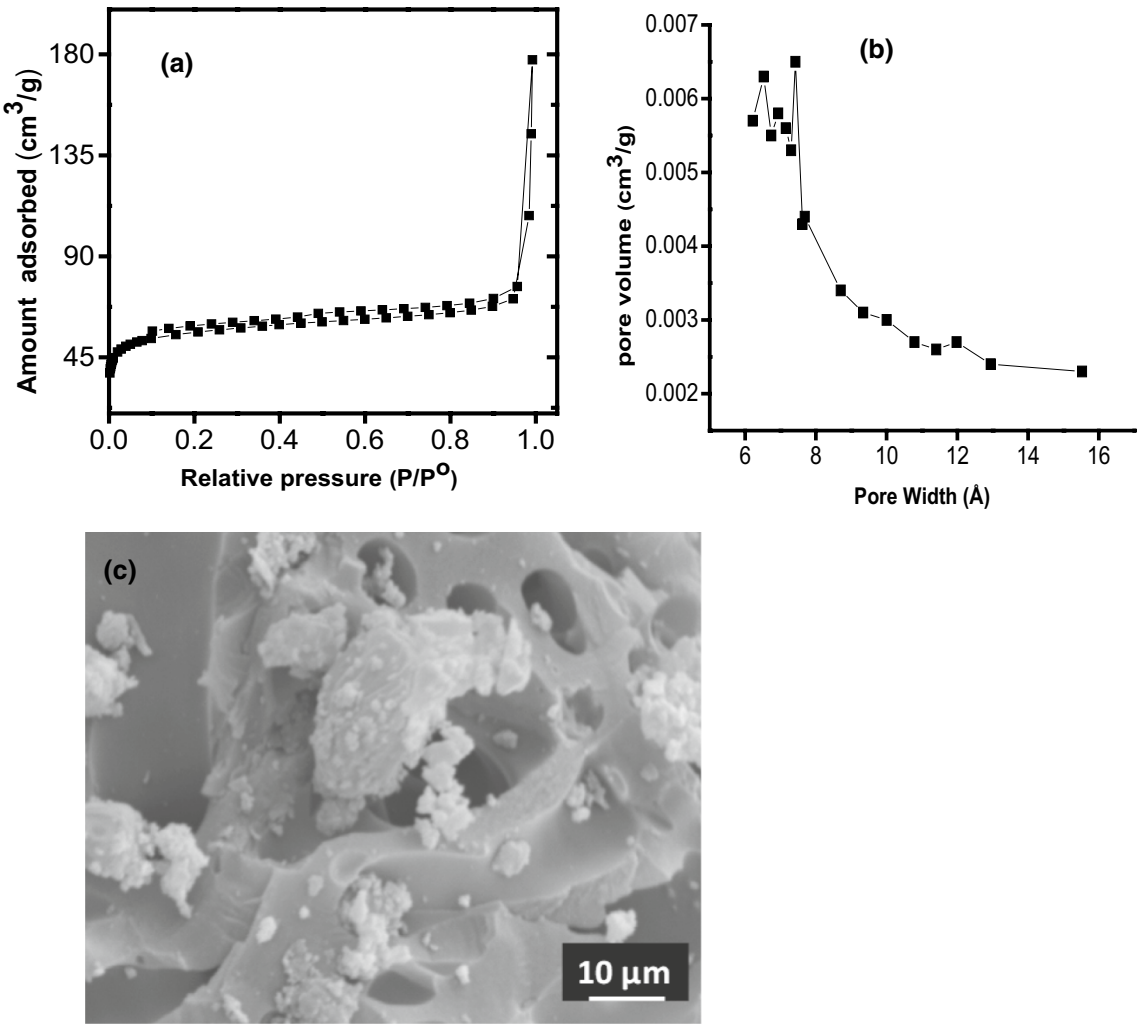

Fig. 2 **a** N_2 adsorption–desorption isotherm, **b** pore size distribution curve (PSD), **c** FESEM micrograph for DES/H_3PO_4-600 2:3

1496 m^2/g, 1436 m^2/g, for ACs that were prepared from Wood sawdust, rayon-based knitted fabrics and coffee. There is also a literature report of lower surface areas adsorbents (Danish et al. 2011; Das et al. 2015; Kyzas and Mitropoulos 2018). Table 1 presents the porous parameters of DES/H_3PO_4 obtained from nitrogen adsorption and the carbon yield. The DES/H_3PO_4 reported a yield of 30.7%.

The FESEM micrographs of DES/H_3PO_4 are shown in Fig. 2c. Evidently, the image shows porous structure that is well developed with large number of cavities of distinct sizes. The various cavities are helpful as they provide the channels for the entrapment of Pb(II) particles. As shown in the figure below, some of the pores were clogged by the H_3PO_4 and could be as a result of unliberated volatiles during the carbonizations process (Usman et al. 2013).

To enable the application and product quality of the DES/H_3PO_4-600 2:3, the thermal stability was investigated by TGA. The TGA curve is presented in Fig. 3a. The AC has three thermal degradation steps within the investigated range, which can be described based on their chemical composition. The first step observed around 100 °C could be ascribed to physically bound water. This was followed by the major weight loss between 200 to 400 °C, where some of the hemicellulose and cellulose were decomposed (Yao et al. 2016). The final stage, which was slow, observed around 400–900 °C, is related to the degradation of lignin in palm kernel shell (Yao et al. 2016). There was about 30% mass loss of the lignin within the investigated temperature. This is against 50% mass loss of the lignin reported by Klapiszewski et al. (2017) using ionic liquids. This shows that the activating agents (DES/H_3PO_4) have a chemical transformation effect on the thermal stability of the biopolymer.

Table 1 Apparent surface area and porosity structural parameters for the DES/H_3PO_4-600 2:3

Adsorbent	AC yield %	Surface area m^2/g	Micropore volume cm^3/g	Total pore volume cm^3/g	Average diameter Å
DES/H_3PO_4-6002:3	30.1	1413	0.5980	0.6181	11.002

For qualitative characterization of surface groups, FTIR spectra were collected and result analysis is presented in Fig. 3b. The spectra of the DES/H_3PO_4-6002:3 contain peaks in the region of 1061, 1158, 1650, 1742, 2900 and 3248 cm^{-1} that are related to C–O group, P=O (in phosphate and polyphosphate) and O–C stretching vibration (in P=OOH and P–O–C linkages), –NH stretching of secondary amine group, C=O, CH and OH stretch vibration (Al-malack and Basaleh, 2016; Danish et al. 2011; Fahmi et al. 2018). With adsorption of Pb onto DES/H_3PO_4-600 2:3, there was a relative change in intensity of the bands and disappearance of some bands compared to the pristine DES/H_3PO_4-600 2:3 (Fig. 3c). This an indication the distorted bands participated to some extent in the removal of Pb(II)ions (Tang et al. 2017). The peak intensity of OH, NH, C=O and phosphate groups obviously increased after adsorption of Pb, which properly could be due to H^+ from carboxyl, hydroxyl or phosphate groups of DES/H_3PO_4-600 2:3 surfaces exchanging with Pb(II) ions, while NH_2, –OH or C=O could provide the needed electrons for surface complexation with Pb(II) ions through formation of coordination bond with oxygen or nitrogen (Huang et al. 2014).

To further elucidate the reactions on the DES/H_3PO_4-600 2:3 surface, the sample was analyzed using XPS. The C1s spectrum of EDS/H_3PO_4 is fit with two peaks

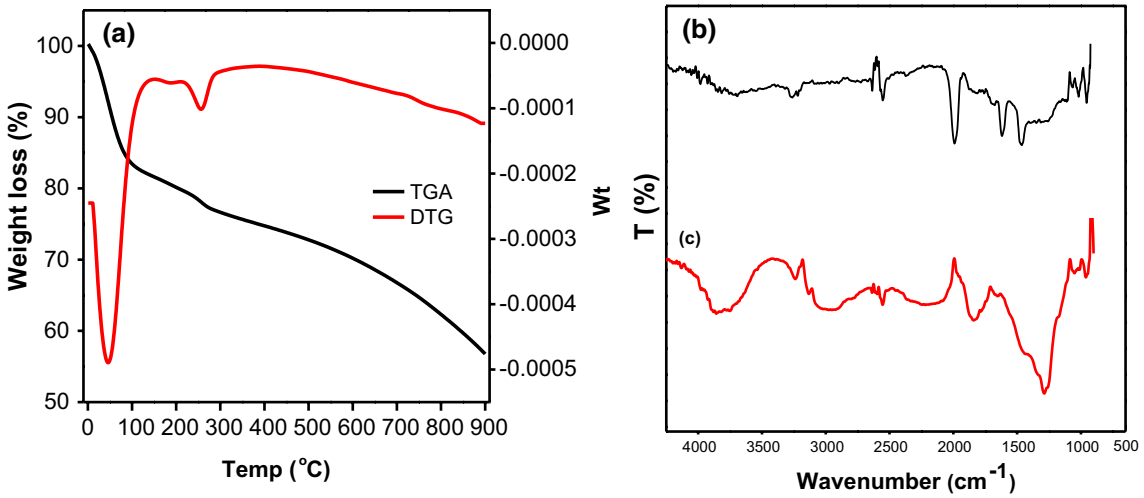

Fig. 3 **a** TGA/DTG analysis curves DES/H_3PO_4-600 2:3 based activated carbon; FTIR of AC-600 2:3, **b** before adsorption, **c** after adsorption

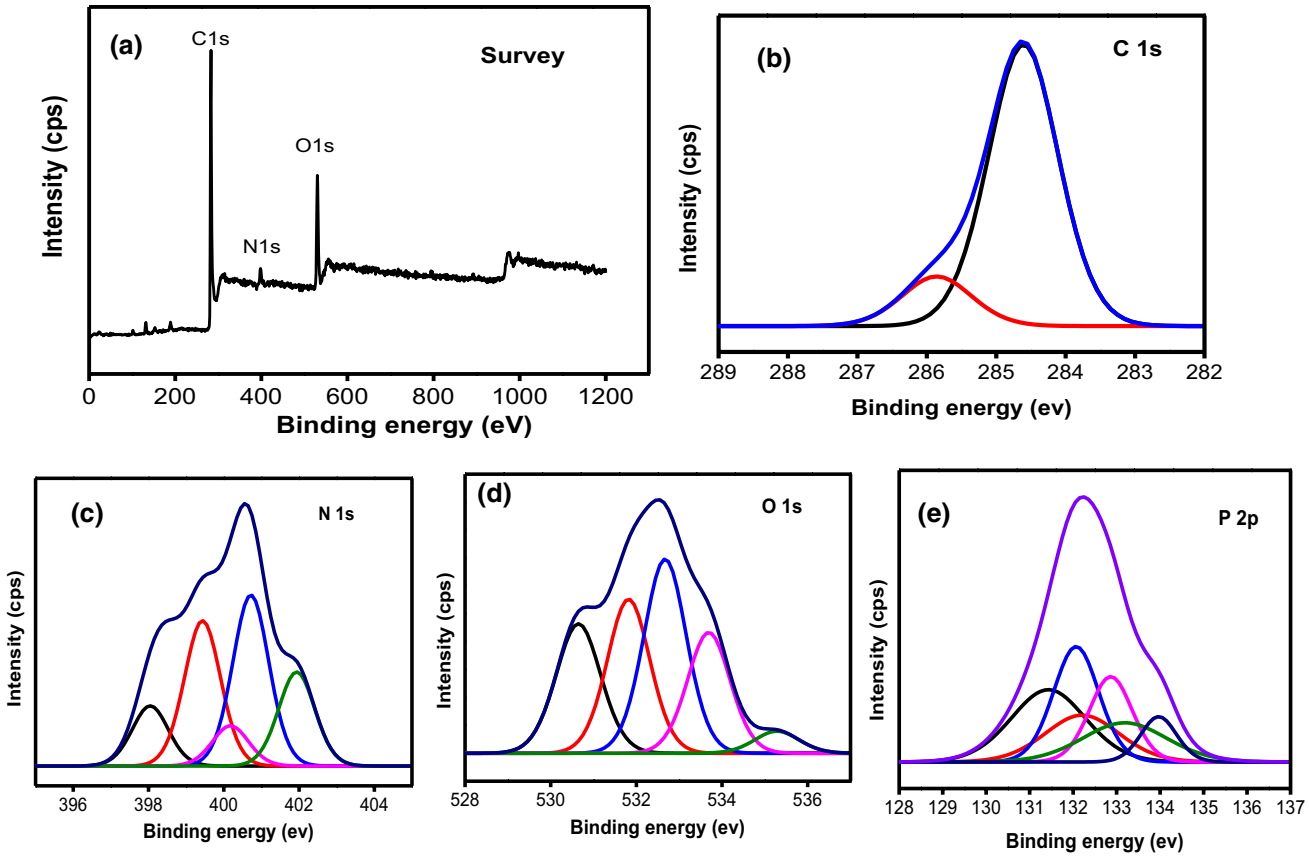

Fig. 4 XPS spectra of EDS/H_3PO_4-600 2:3. **a** wide scan, **b** C 1s spectra, **c** N 1 s spectra, **d** O 1s spectra and **e** P 2p spectra

at 284.6 and 285.7 eV (Fig. 4a), allotted to adventitious carbon(C–C/C=C)(Liu et al. 2018a, b, c) and C–H species (Kapilov-Buchman et al. 2017), respectively. The band gotten by spectra deconvolution O1s is presented in Fig. 4d. The peak positioned at 532.0 eV is attributed to C–O and/or P–O bonds(Zhao et al. 2014), while 530.5 (C=O in quinones), 532.7 (chemisorbed H_2O) (Li et al. 2015), 533.2 eV (P–O–P bonds)(Li et al. 2015) and 534.3 (COH, –COOH, –N–O–N–)(Li et al. 2014). The fitting curve analysis for N1s band was resolved into four peaks. The binding energies at 398.4, 399.4, 400.1, 400.8 and 401.9 eV are attributed pyridinic nitrogen (Chen et al. 2018; Kapilov-Buchman et al. 2017), –N=C group (Yang et al. 2012), pyrrolic nitrogen (Chen et al. 2018), graphitic nitrogen (Kapilov-Buchman et al. 2017) and graphitic2 nitrogen (Kiuchi et al. 2016). Curve fitting analysis for P 2p shows main component with BE = 131.4–133.9 eV ascribed to phosphate species on the DES/H_3PO_4-600 2:3 surfaces related to P-atom bonded to O and C-atoms or phosphate-likes structures, which agrees with the FTIR result. Besides, the P 2p spectrum was resolved into five components. The band energy at 133.50 represents P=O (L. Liu et al. 2018a, b, c), the two peaks at 131.4 and 132.8 eV binding energy are related to the P–C bonding (Hou et al. 2017; J. Wang et al. 2018), while peaks at 133.1 and 133.9 eV binding energy correspond P–O (Liu et al. 2018a, b, c; Wang et al. 2018).

The functional groups on DES/H_3PO_4-600–2:3 would give rise to the adsorption properties of the biosorbent. Oxygen-containing groups (–OH,–COOH,–ROH) and nitrogen functional groups (Mi et al. 2019) of adsorbents surfaces, apart from surface area and pore volume, contribute significantly to the adsorption process. Moreover, both pyridinic nitrogen and pyrrolic nitrogen (Mi et al. 2019) and phosphate groups (Liu et al. 2018a, b, c) on the adsorbents are reported to influence heavy metal ion removal. It is expected that the properties of DES/H_3PO_4-600 2:3, including porosity, functional groups would have had influential effect on the efficacy of DES/H_3PO_4-600 2:3 during the adsorption of Pb(II) ions from aqueous solution. Moreover, changes observed after adsorption of lead on the FTIR could be an indication of some of these functional groups participating in removal of Pb(II) ions.

Adsorption characteristics of lead on DES/H_3PO_4-600 2:3

DES/H_3PO_4-600 2:3 dosage

In order to ascertain removal capacity of DES/H_3PO_4-600 2:3 for a given lead initial concentration in aqueous solution, the effect of adsorbent dosage was examined. It can be seen that increase in adsorbent dosages concentration in the range 0.1 to 0.3 g leads to significant increase in active sites concentration, leading to a corresponding removal efficiency of Pb(II) from 36.0 to 50%. However, a decreasing trend in the adsorbed amount of Pb per unit mass of DES/H_3PO_4-600 2:3 from 38.1 to 16.6 mg/g was observed by the same dosage variation, which could be attributed to unsaturation sorption sites present on the adsorbent due to decrease in the quantity of Pb(II) to available sorption sites. The effect of varying DES/H_3PO_4-600 2:3 dosage on Pb(II) removal is shown in Fig. 5**.** Thus, considering efficiency and economy (Liu et al. 2018a, b, c), we considered 0.20 g/mL as optimum DES/H_3PO_4-600 2:3 load to assess the effect of other parameters in later experiments.

Effect of concentration and contact time

The effect of initial concentration on the adsorption of Pb(II) onto DES/H_3PO_4-600 2:3 was examined by varying initial concentrations from 75 to 150 mg/L using adsorbent dosage of 0.2 g. Varying the concentration from 75 to 150 mg/L, the uptake amount of Pb(II) adsorbed increased from 40 to 62.8 mg/g. As observed in Fig. 6, the uptake rate of Pb(II) was concentration dependent and DES/H_3PO_4-600 2:3 had superior removal capacity at the highest concentration investigated. This is because higher concentrations provide the needed driving force that is high enough to repress the mass transfer barrier between DES/H_3PO_4-600 2:3 and the aqueous phase. Similar phenomenon could be observed for adsorption of Pb(II) on potato peels (Kyzas and Mitropoulos 2018). Additionally, the sorption rate of Pb(II) ions was rapid at first 80 min and then becomes almost constant as the removal process proceeds. The sorption rate could be seen to be initially fast at the beginning of the experiment due to the accessibility of large number of sorption sites, but as the reaction proceeds, slower uptake could be observed due to the decrease in available sorption sites on DES/H_3PO_4-600 2:3. Hence, the equilibrium time at 120 min can be considered to be sufficient enough for the removal of Pb(II) by DES/H_3PO_4-600 2:3 from water.

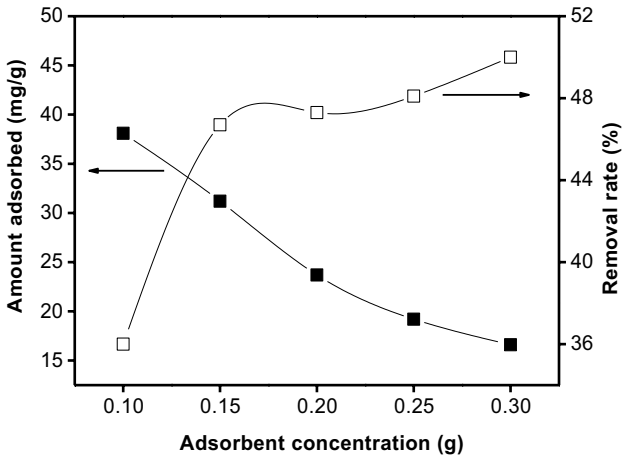

Fig. 5 The effect of DES/H_3PO_4-600 2:3 dosage on adsorption Pb(II) ($[Pb]_o$ = 50 mg/L, time = 1 h.30 min

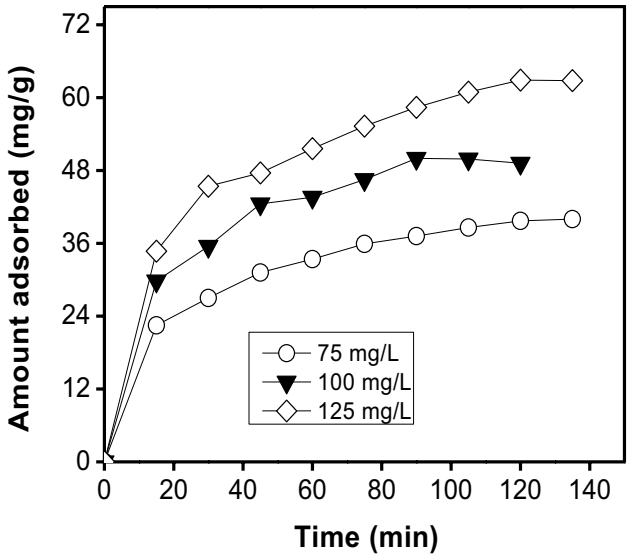

Fig. 6 Adsorption of Pb(II) on DES/H_3PO_4-600–2:3 as a function of initial concentration (dosage = 0.2 g/L)

Effect of solution pH on the removal of Pb(II*)*

pH remains a dominant factor that controls uptake capacity of metal ions from solution(Wang et al. 2011a, b). Figure 7 illustrates the effect of pH on Pb uptake. Increasing the pH values from 1–6, Pb(II) adsorption on to DES/H_3PO_4-600 2:3 increased steadily and attained a maximum peak at a pH value of 5 and afterward deceased. The decrease in sorption rate of Pb(II) at pH < 5 can be traced to the abundant of H^+ that competes with Pb(II) for the available negative binding sites on DES/H_3PO_4-600 2:3. As the solution pH increased, the DES/H_3PO_4-600 2:3 surface charge increased inversely to pH, which reduces H^+ competition for available binding sites with Pb(II). Consequently, maximum uptake capacity of DES/H_3PO_4-600 2:3 was 73.5 mg/g, which was reported at initial pH value of 5.0, and could be attributed to electrostatic attraction between the negatively charged surface of the DES/H_3PO_4-600 2:3 and positively charge Pb(II).

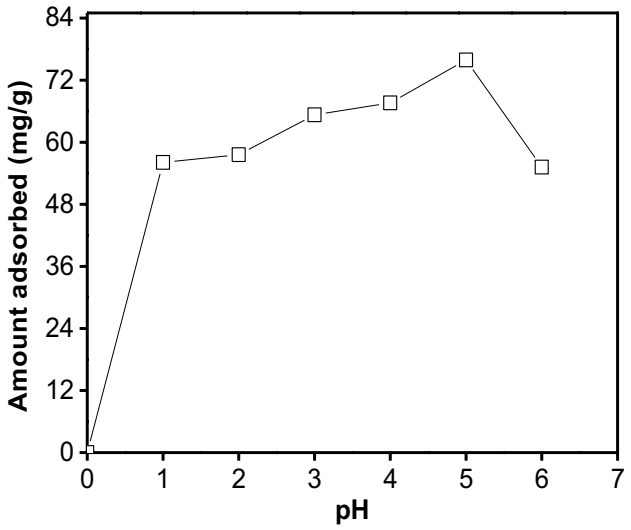

Fig.7 Effect of initial pH on Pb(II) adsorption ($[Pb]_o = 125$ mg/L, adsorbent dosage = 0.2 g/L, time = 120 min, T = 25 ± 2 °C)

These observations are similar to what has been previously reported about Pb(II) adsorption onto biosorbent. Precisely, Kolodyńska et al. (2017) and Liu et al. (2018a, b, c) achieved maximum efficiency by varying initial pH to 5. When the initial pH was > 5, the removal efficiency of Pb(II) decreased as a result of $Pb(OH)^+$ and/or $Pb(OH)_2$ (soluble hydroxyl complexes) (Alghamdi et al. 2019). Moreover, at pH > 6, Pb will precipitate out of solution(Liu et al. 2018a, b, c), and Pb^{2+} and $Pb(OH)^+$ are the dominant Pb species at pH ranging from 5–7.5, but when the solution pH is > 7.5, $Pb(OH)^+$ reportedly turn to $Pb_2(OH)(OH)_4{}^{2+}$ (Sharaf El-deen and Sharaf El-deen 2016). Thus, all subsequent adsorption studies involving pH were operated at pH 5.

Adsorption isotherm and sorption kinetics

Adsorption isotherm model was used to describe the relationship between equilibrium concentrations of the adsorbate and the adsorption capacity of the adsorbent (Ali et al. 2019). In the present study, Langmuir (Eq. 1) and Freundlich (Eq. 2) isotherms were tested to analyze the sorption behavior of Pb(II) by DES/H_3PO_4-600 2:3.

$$C_e/q_e = 1/Q_{\max}b + C_e/Q_{\max} \tag{4}$$

$$\mathrm{In}q_e = \mathrm{In}K_F + (1/\mathrm{n})\mathrm{In}C_e \tag{5}$$

where C_e and q_e are equilibrium concentration of Pb in solution (mg/L) and equilibrium uptake (mg/g), respectively. $Q_{\max}$ is the maximum theoretical monolayer adsorption capacity of the adsorbent (mg/g), while b is related to energy of adsorption. n and K_F (mg/g (L/mg)$^{1/n}$) are linked to the adsorption capacity and favorability of the removal process, respectively. The Langmuir constants $Q_{\max}$ and b were calculated from the slope and intercept of a liner plot of C_e/Q_e versus C_e (Fig. 8a), while the Freundlich constants (n and K_F) were obtained from the slop and intercept of liner plot of $\mathrm{In}q_e$ versus $\mathrm{In}C_e$ (Fig. 8b). The related parameters of the isotherms are presented in Table 3. Judging on the basis of correlation coefficients (R^2) and $Q_{\max}$ values, the Langmuir isotherm model revealed more satisfactory results with $R^2 > 0.9$ as compared to the Freundlich model with $R^2 < 0.7$, and could be traced to binding sites that are uniformly distributed on DES/H_3PO_4-600 2:3. The $Q_{\max}$ for DES/H_3PO_4-600 2:3 was 98.3 mg/g. Compared to other adsorbents, the DES/H_3PO_4-600 2:3 demonstrated good adsorption properties. The $Q_{\max}$ for Pb(II) adsorption was revealed to be 21.38, 49.92, 50.00, 63.29—89.28, 90.0 mg/g from different activated carbons obtained from apricot stone, coconut shell, polypyrrole-based AC, coffee residue AC and municipal organic solid waste, respectively, and in previous studies (Table 2) were below that of DES/H_3PO_4-600 2:3. This result revealed that AC prepared by cleaner method using PKS and DES/H_3PO_4 activating agent is promising, especially for the treatment of Pb in water. The high removal capacity reported by EDS/H_3PO_4-600 2:3 could be linked to its ordered pore structure and available function groups on the surface. Equally, maximum adsorption capacity of DES/H_3PO_4-600 2:3 was compared to materials with significantly better parameters (Table 2). To quantify the adsorption rate information, the data reported from the kinetic experiment were described by kinetic equations (Eqs. 6 and 7), respectively, and both the removal rate and removal capacity could be a function of the adsorbent properties (e.g., surface area, porosity, aromaticity, etc.) (Abdallah et al. 2019). Pseudo-first-order model assumes that the removal rate is dependent on adsorption capacity, whereas the pseudo-second-order is controlled by chemisorption (i.e., involves sharing of electron pairs between the adsorbent and adsorbate (Alghamdi et al. 2019).

$$\log(q_e - q_t) = \log - \left(\frac{k_1}{2.303}\right) \tag{6}$$

$$t/q_t = 1/k_2 q_e^2 + t/q_e \tag{7}$$

where K_1 (min^{-1}) and K_2 (g/mg.min) are rate constants for pseudo-first-order and pseudo-second-order, respectively. Also, q_t and q_e are the amount of Pb(II) adsorbed per mass of DES/H_3PO_4-600 2:3 at any given time t(min) and at equilibrium, respectively. When $\log(q_e\text{-}q_t)$ vs t and t/q_t vs t is plotted, K_1, K_2 and q_e are obtained from the intercept and slope. The liner equation fitted by kinetic models (pseudo-first- and

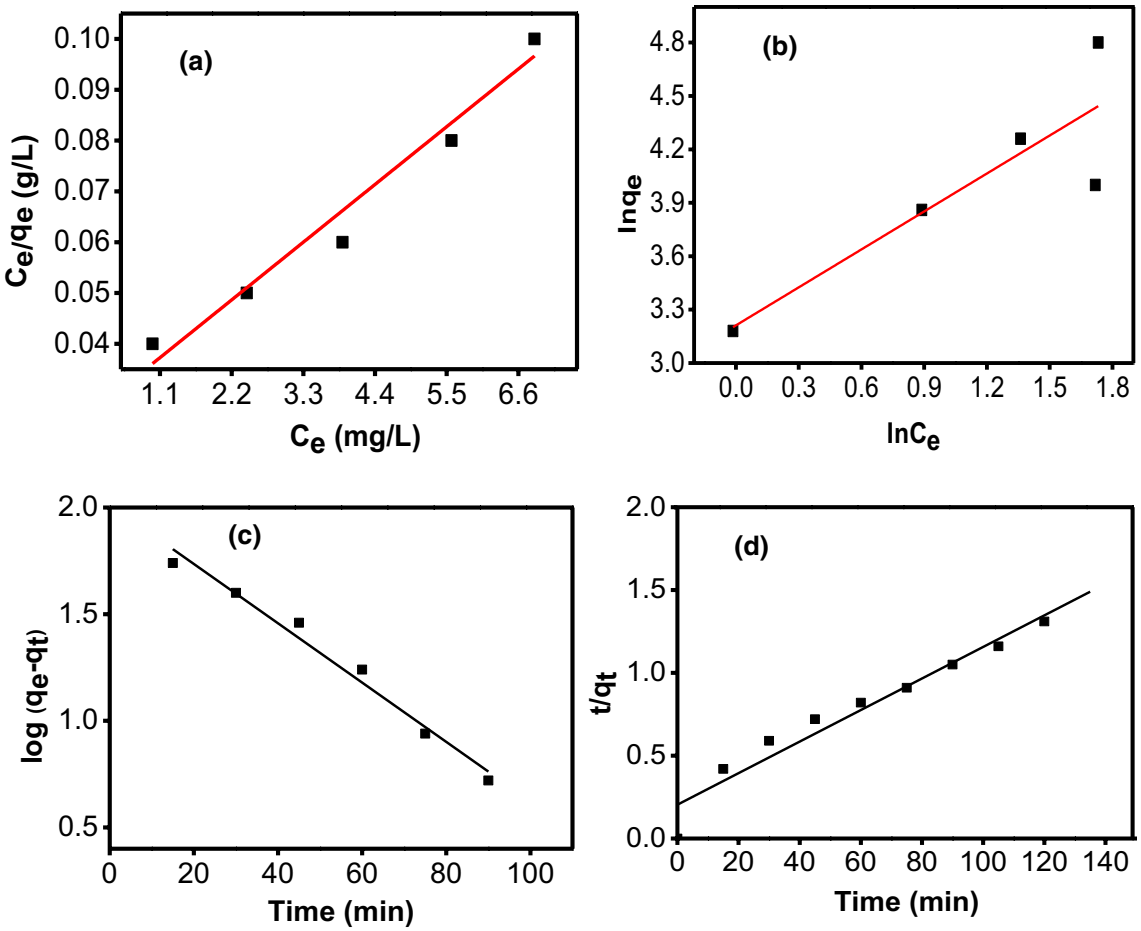

Fig. 8 Adsorption isotherm model of Pb(II) adsorption. **a** Langmuir; **b** Freundlich ($[Pb]_o = 25$, 50, 75, 100 and 125 mg/L); **c** pseudo-first-order kinetic plot; **d** pseudo-second -order kinetic plot for the adsorption of Pb(II) ($[Pb]_o = 125$ mg/L; dosage = 0.2 g/L; time = 140 min; temp. = 25 ± 2 °C)

Table 2 Parameters for the adsorption of Pb(II) by DES/H_3PO_4-600 2:3 according to Isotherm and kinetic models

Isotherm						
Langmuir				Freundlich		
Q_m (mg/g)	b (L/mg)	R_L	R^2	1/n	K_F (mg/g)(L/mg)n	R_2
97.1	0.0481	0.1424	0.9681	1.2565	1.2790	0.6565
Kinetics study						
Pseudo-first order				Pseudo-second order		
Q_e exp (mg/g)	Q_e cal (mg/g)	k_1 (min^{-1})	R^2	Q_e cal (mg/g)	K_2(g/mg min)	R^2
96.7	39.5	0.030	0.8209	96.1	0.068	0.9999

pseudo-second-order models) is presented in Fig. 8c-d, and the computed parameters are listed in Table 3. The adsorption process onto DES/H_3PO_4-600 2:3 followed second-order rate equation. As can be seen from the table, the values calculated from the model showed correlation coefficient (R^2) value closer to satisfactory (0.9999) with theoretically calculated q value ($q_{e,cal}$) in good agreement with experimental value ($q_{e,\,exp}$). These findings indicated that chemisorption mechanism is the rate-limiting step.

Table 3 Adsorption capacity of various adsorbents compared with DES/H_3PO_4-600 2:3

Adsorbents	Activating Agent	S_{BET} (m^2/g)	Total pore volume (cm^3/g)	Q_{max} (mg/g)	Reference
PKS	DES/H_3PO_4	1413	0.618	97.07	This study
Polypyrrole	KOH	2871	0.054	50.00	Alghamdi et al., 2019
Apricot stone	H_2SO_4	393	0.192	21.38	Mouni et al., 2011
Composite	TiO_2/CF	14.95		42.5	Zhang et al, 2016
Winemaking Waste	KOH	1194	1.4	58	Alguacil et al., 2018
Coconut shell	H_3PO_4	624		49.92	Sharaf El-deen & Sharaf El-deen, 2016
Coffee residue	H_3PO_4	1003	0.618	89.28	Boudrahem et al., 2011
Coffee residue AC	$ZnCl_2$	858	0.549	63.29	Boudrahem et al., 2011
MOSW AC	H_3PO_4	790	0.523	90.0	Al-malack & Basaleh, 2016
Chickpea husk	KOH & K_2CO_3	2082	1.070	135.8	Özsin et al., 2019
Milkweed AC	–	170	1.07	316.3	Ilangovan et al., 2017

MOSW = municipal organic solid waste

Effect of temperature and thermodynamics studies

Changes in adsorption capacity for the removal process of Pb(II)ions were investigated in the temperature range of 30 to 50 °C. As seen in Fig. 9a, the removal rate for Pb(II) decreased from 90.8 to 54.5 mg/g as the solution temperatures increased. The result demonstrated that the adsorption process of DES/H_3PO_4-600 2:3 for the treatment of Pb(II) in solution is exothermic. Hence, a decrease in solution temperature will be more beneficial to the adsorption of Pb(II). Furthermore, the data obtained from the effect of solution temperature were used to describe the pertinent thermodynamic parameters such as ΔG^o (Gibbs free energy) (obtained from Eq. 8), ΔH^o (enthalpy) and ΔS^o(entropy), both calculated Vant Hoff's equation (Eq. 9).

$$\Delta G^o = -\mathrm{RT}\ln K_C \tag{8}$$

$$\ln K_C = \left(\frac{\Delta S}{R}\right) - \left(\frac{\Delta H}{R}\right)\frac{1}{T}. \tag{9}$$

K_c is the distribution coefficient, otherwise called the thermodynamic equilibrium constant and was evaluated using.

$$K_C = \frac{C_o - C_e}{C_e} \tag{10}$$

where C_e is the amount of Pb(II) on DES/H_3PO_4-600 2:3 (mg/g), C_o–C_e defines the equilibrium concentration of Pb(II) in solution (mg/L), whereas the gas constant is represented by R. By increasing solution temperature from 30

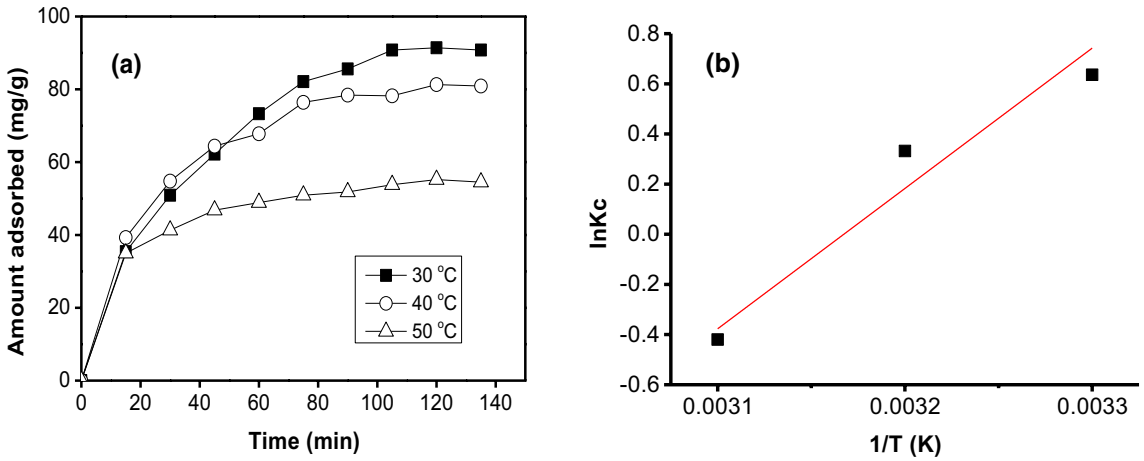

Fig. 9 **a** Adsorption of Pb(II) by DES/H_3PO_4-600 2:3 as a function of temperature, **b** Vant Hoff's plot.(dosage = 0.2 g/L, time = 140 min, $[Pb]_o$ = 125 mg/L, pH = 5)

to 50 °C, the ΔG^o values became less negative (− 1.612, − 0.858 and 1.127 kJ/mol), indicating the spontaneity of the adsorption process of DES/H_3PO_4-600 2:3 for Pb(II) and its feasibility at lower temperature. At 50 °C, we reported a positive value of ΔG^o, indicating a non-spontaneous process at this temperature. This result is in agreement with the ΔH (− 43.90 kJ/mol) confirming the exothermic natures of the adsorption process (Liu et al., 2020), which also supported by the changes in uptake capacity for Pb(II) removal. Equally, the ΔS^o value was < 0 (− 138.95 J/Kmol) signifying a decrease in randomness (Liu et al., 2020) at the DES/H_3PO_4-600 2:3/aqueous interphase in the course of the adsorption process.

Competitive adsorption

Single and binary adsorption systems are vital in estimating the efficacy of DES/H_3PO_4-600 2:3 for Pb(II) removal in wastewater. Heavy metals are known to coexist; their interaction with each other and other components in the water ecosystem has adversative effect on their transport at the solid/aqueous phase interfaces (Park et al. 2016). Consequently, we investigated the adsorption process of DES/H_3PO_4-600 2:3 for Pb(II) in the presence of Cu(II). By using the removal ratio (i.e., amount adsorbed in bimetal component (q_e) to the amount adsorbed in a single component (Q_m)), we were able to estimate the effect of binary metal solution on the adsorption process of DES/H_3PO_4-600 2:3. When $Q_e/Q_m > 1$, adsorption is synergistic, when $Q_e/Q_m = 1$, adsorption is non-interactive, and when $Q_e/Q_m < 1$, adsorption is antagonistic. As seen in Fig. 10, the adoption ratio values in the bimetal solution adsorption were < 1 (Pb-Cu = 0.87 and Cu-Pb = 0.66), indicating antagonistic effect of one metal over the other. Pb(II) has shown greater antagonistic effect over Cu(II), with a sorption maxima that is reportedly inversely proportional to the hydrated ionic radii of the metal (Pb(II) = 4.01 Å > Cu(II) 4.19 Å (Chen et al. 2010) and relative positions in the electrochemical series (Abu-nada et al. 2020). These results conform to other studies from Bansode et al. (2003) on pecan shell-based granular activated carbons, Sitko et al. (2013) on graphene oxide, and Xie et al. (2013) on sludge-based AC. However, this trend is contrary to adsorption pattern of Cu > Pb reported by Yantasee et al. (2004) on fine-grained AC functionalized with amine, and Li et al. (2016) on banana peels. This can be attributed to various sorption sites (hydrophobic or nonionic versus ionic) that are less dependent on cation electronegativity on these activated carbons (fine-grained AC functionalized with amine and banana peels) (Bansode et al. 2003) compared to the PKS-based AC investigated in this work.

Reusability studies

In order to establish the stability potential and economic viability of DES/H_3PO_4-600 2:3 in water treatment, a reusability study was conducted using adsorption–desorption experiments in batch mode for three cycles. The preused DES/H_3PO_4-600 2:3 was agitated for 2 h with 0.1 HNO_3 to detach the adsorbed Pb(II) on the surfaces, then ultrasonicated for 15 min and then washed several times with deionized water and dried, before repeatedly used to adsorb Pb(II) from solution. The regenerated result for DES/H_3PO_4-600 2:3 of 3 cycles is shown in Fig. 11. The result reveals that there was a little reduction in the removal amount from the first to the third cycle compared to the fresh adsorbent by about 7%. The desorption experiments have demonstrated that DES/H_3PO_4-600 2:3 had potential for efficient remediation of Pb(II) in water and a probably renewable adsorbent.

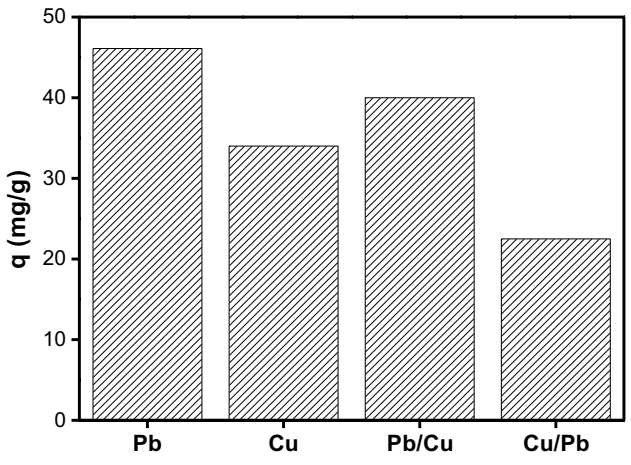

Fig. 10 Adsorption of Pb(II) by DES/H_3PO_4-600 2:3 as function of the co-cations in solution (Time = 120 min, pH = 5, Temp. = 25 ± 2 °C)

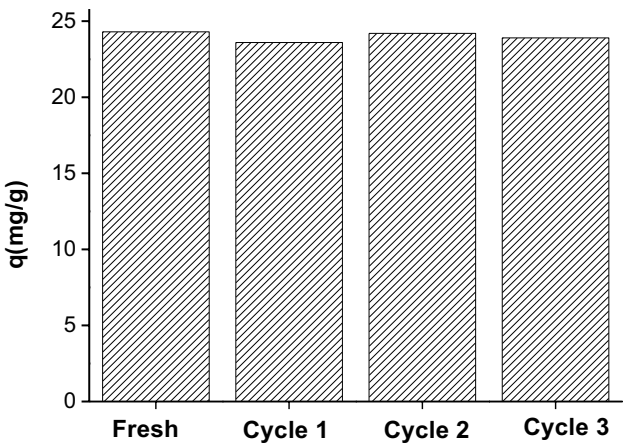

Fig. 11 Effect of regeneration of DES/H_3PO_4-600 2:3 on adsorption capacity

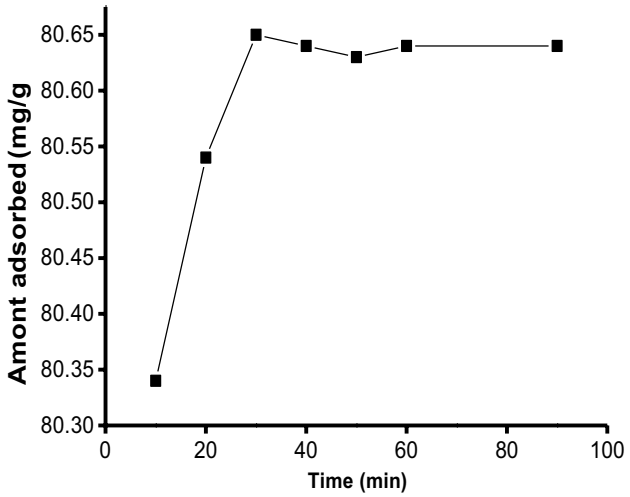

Fig. 12 Fitting curve for Pb(II) adsorption onto DES/H_3PO_4-600 2:3 from real industrial wastewater(dosage = 0.2 g/L, $[Pb]_o$ = 81.0 mg/L, T = 30 °C, pH = 5)

Real wastewater treatment

The chemical composition of an effluent from an industrial discharge may differ largely to the synthetic wastewater, as an appraisal of the results of the present study for application to a real wastewater treatment, the use of an industrial wastewater sample was proposed. For this purpose, wastewater collected from an industrial plant was investigated. The wastewater sample, which contained up to 81.0 mg/L, was treated using DES/H_3PO_4-600 2:3. The result from the analysis of the effluent using atomic adsorption spectrometer showed that DES/H_3PO_4-60 2:3 was capable to reducing the amount of Pb(II) in the effluent to below 0.5 mg/L, though, above 100 min of treatment, the concentration of Pb(II) in the effluent was lower than the detection limit of the instrument. The result has demonstrated that DES/H_3PO_4-600 2:3 is a promising alternative for the treatment of Pb(II) from real wastewater. The removal profile for the treatment of Pb(II) from the effluent using DES/H_3PO_4-600 2:3 is shown in Fig. 12

Conclusions

We have demonstrated a new approach in the preparation of a low-cost AC, using inexpensive PKS and eco-friendly DES/H_3PO_4, for a high efficient adsorbent with a green chemical framework for the treatment of Pb in water. The EDS/H_3PO_4-600 2:3 showed good porous structure and large surface area (1413 m^2/g), resulting in satisfactory adsorption of Pb(II). The XPS and FTIR characterization revealed the oxygen-containing groups on EDS/H_3PO_4-600 2:3 due to activation of DES/H_3PO_4 which played a vital role in the removal Pb(II) ions. The result indicated that increasing the initial concentration and the pH value increases the amount removal. The adsorption test was well described by Langmuir model and pseudo-second-order kinetic equation. Meanwhile, increasing the solution temperature decreased the adsorption capacity of the prepared DES/H_3PO_4-600 2:3. The negative value of the enthalpy ΔH (− 43.90 kJ/mol) showed that the adsorption process of Pb(II) on DES/H_3PO_4-600 2:3 was exothermic and spontaneous under the condition investigated.

The novelty of this work is that applying DES/H_3PO_4 as an activating agent gives a good ordered activated carbon structure that has significantly promoted adsorption and offers a practical benign/cleaner production approach in the synthesis of activated carbon with good reusability and good wastewater purification ability. To ensure process sustainability, future studies will be focused on long-term pilot studies using column for potential scale-up and revealing the competitive effect of other metals on Pb removal in column.

Funding This research received no external funding.

Declarations

Conflicts of interest The authors declare that they have no conflict of interest.

References

Abdallah MM, Ahmad MN, Walker G, Leahy JJ, Kwapinski W (2019) Batch and continuous systems for Zn, Cu, and Pb metal ions adsorption on spent mushroom compost biochar. Ind Eng Chem 58(17):7296–7307. https://doi.org/10.1021/acs.iecr.9b00749

Abu-Nada A, McKay G, Abdala A (2020) Recent advances in applications of hybrid graphene materials for metals removal from wastewater. Nanomaterials 10(3):595

Ahmed MB, Johir MAH, Zhou JL, Ngo HH, Nghiem LD, Richardson C, Moni MA, Bryant MR (2019) Activated carbon preparation from biomass feedstock: clean production and carbon dioxide adsorption. J Cleaner Prod 225:405–413. https://doi.org/10.1016/j.jclepro.2019.03.342

Alghamdi AA, Al-Odayni AB, Saeed WS, Al-Kahtani A, Alharthi FA, Aouak T (2019) Efficient adsorption of lead(II) from aqueous phase solutions using polypyrrole-based activated carbon. Materials 12(12):2020

Alguacil FJ, Alcaraz L, García-Díaz I, López FA (2018) Removal of Pb^{2+} in wastewater via adsorption onto an activated carbon produced from winemaking waste. Metals 8(9):697. https://doi.org/10.3390/met8090697

Ali IH, Al Mesfer MK, Khan MI, Danish M, Alghamdi MM (2019) Exploring adsorption process of lead(II) and chromium(VI) ions from aqueous solutions on acid activated carbon prepared from Juniperus procera leaves. Processes 7(4):217

Al-Malack MH, Basaleh AA (2016) Adsorption of heavy metals using activated carbon produced from municipal organic solid waste. Desalin Water Treat 57(51):24519–24531. https://doi.org/10.1080/19443994.2016.1144536

Bansode RR, Losso JN, Marshall WE, Rao RM, Portier RJ (2003) Adsorption of metal ions by pecan shell-based granular activated carbons. Bio Tech 89(2):115–119. https://doi.org/10.1016/S0960-8524(03)00064-6

Boskabady M, Marefati N, Farkhondeh T, Shakeri F, Farshbaf A, Boskabady MH (2018) The effect of environmental lead exposure on human health and the contribution of inflammatory mechanisms, a review. Environ Int 120:404–420. https://doi.org/10.1016/j.envint.2018.08.013

Boudrahem F, Soualah A, Aissani-Benissad F (2011) Pb (II) and Cd (II) removal from aqueous solutions using activated carbon developed from coffee residue activated with phosphoric acid and zinc chloride. J Chem Eng Data 56(5):1946–1955

Carriazo D, Gutiérrez MC, Picó F, Rojo JM, Fierro JL, Ferrer ML, del Monte F (2012) Phosphate-functionalized carbon monoliths from deep eutectic solvents and their use as monolithic electrodes in supercapacitors. Chemsuschem 5(8):1405–1409. https://doi.org/10.1002/cssc.201200136

Chen SB, Ma YB, Chen L, Xian K (2010) Adsorption of aqueous Cd^{2+}, Pb^{2+}, Cu^{2+} ions by nano-hydroxyapatite: single-and multi-metal competitive adsorption study. Geochem J 44(3):233–239. https://doi.org/10.2343/geochemj.1.0065

Chen F, Xie S, Huang X, Qiu X (2017) Ionothermal synthesis of Fe_3O_4 magnetic nanoparticles as efficient heterogeneous Fenton-like catalysts for degradation of organic pollutants with H_2O_2. J Hazard Mater 322:152–162. https://doi.org/10.1016/j.jhazmat.2016.02.073

Chen L, Deng J, Hong S, Lian H (2018) Deep eutectic solvents-assisted cost-effective synthesis of nitrogen-doped hierarchical porous carbon xerogels from phenol-formaldehyde by two-stage polymerization. J Sol-Gel Sci Techn 86(3):795–806. https://doi.org/10.1007/s10971-018-4660-8

Dai YD, Shah KJ, Huang CP, Kim H, Chiang PC (2018) Adsorption of nonylphenol to multi-walled carbon nanotubes: Kinetics and isotherm study. Appl Sci 8(11):1–13. https://doi.org/10.3390/app8112295

Danish M, Hashim R, Ibrahim MM, Rafatullah M, Ahmad T, Sulaiman O (2011) Characterization of Acacia mangium wood based activated carbons prepared in the presence of basic activating agents. BioResources 6(3):3019–3033. https://doi.org/10.4172/2157-7048.1000248

Das D, Samal DP, Meikap BC (2015) Preparation of activated carbon from green coconut shell and its characterization. J Chem Eng Process Technol. https://doi.org/10.4172/2157-7048.1000248

Di Gioia ML, Nardi M, Costanzo P, De Nino A, Maiuolo L, Oliverio M, Procopio A (2018) Biorenewable deep eutectic solvent for selective and scalable conversion of furfural into cyclopentenone derivatives. Molecules 23(8):1891. https://doi.org/10.3390/molecules23081891

Edokpayi JN, Odiyo JO, Msagati TA, Popoola EO (2015) A Novel Approach for the removal of lead (II) ion from wastewater using mucilaginous leaves of diceriocaryum eriocarpum plant. Sustainability 7(10):14026–14041. https://doi.org/10.3390/su71014026

Fahmi AH, Samsuri AW, Jol H, Singh D (2018) Physical modification of biochar to expose the inner pores and their functional groups to enhance lead adsorption. RSC Adv 8(67):38270–38280. https://doi.org/10.1039/c8ra06867d

Fenga C, Gangemi S, Di Salvatore V, Falzone L, Libra M (2017) Immunological effects of occupational exposure to lead. Mol Med Rep 15(5):3355–3360. https://doi.org/10.3892/mmr.2017.6381

Fiyadh SS, AlOmar MK, Binti Jaafar WZ, AlSaadi MA, Fayaed SS, Binti Koting S, Lai SH, Chow MF, Ahmed AN, El-Shafie A (2019) Artificial neural network approach for modelling of mercury ions removal from water using functionalized CNTs with deep eutectic solvent. Int J Mol Sci 20(17):4206

Foo KY, Hameed BH (2012) Mesoporous activated carbon from wood sawdust by K_2CO_3 activation using microwave heating. Bioresour Technol 111:425–432. https://doi.org/10.1016/j.biortech.2012.01.141

He Y, Wu P, Xiao W, Li G, Yi J, He Y, Chen C, Ding P, Duan Y (2019) Efficient removal of Pb (II) from aqueous solution by a novel ion imprinted magnetic biosorbent: adsorption kinetics and mechanisms. PLoS ONE 14(3):1–17. https://doi.org/10.1371/journal.pone.0213377

Hou H, Shao L, Zhang Y, Zou G, Chen J, Ji X (2017) Large-area carbon nanosheets doped with phosphorus: a high-performance anode material for sodium-ion batteries. Adv Sci 4(1):1600243. https://doi.org/10.1002/advs.201600243

Huang Y, Li S, Lin H, Chen J (2014) Fabrication and characterization of mesoporous activated carbon from Lemna minor using one-step H_3PO_4 activation for Pb (II) removal. Appl Surf Sci 317:422–431. https://doi.org/10.1016/j.apsusc.2014.08.152

Huang Y, Wang Y, Pan Q, Wang Y, Ding X, Xu K, Li N, Wen Q (2015) Magnetic graphene oxide modified with choline chloride-based deep eutectic solvent for the solid-phase extraction of protein. Anal Chim Acta 877:90–99. https://doi.org/10.1016/j.aca.2015.03.048

Ilangovan M, Guna V, Olivera S, Ravi A, Muralidhara HB, Santosh MS, Reddy N (2017) Highly porous carbon from a natural cellulose fiber as high efficiency sorbent for lead in waste water. Bioresour Technol 245:296–299. https://doi.org/10.1016/j.biortech.2017.08.141

Inamuddin, Ismail YA (2010) Synthesis and characterization of electrically conducting poly-o-methoxyaniline Zr(1V) molybdate Cd(II) selective composite cation-exchanger. Desalination, 250(2):523–529. https://doi.org/10.1016/j.desal.2008.06.033

Jan AT, Azam M, Siddiqui K, Ali A, Choi I, Haq QM (2015) Heavy metals and human health: mechanistic insight into toxicity and counter defense system of antioxidants. Int J Mol Sci 16(12):29592–29630. https://doi.org/10.3390/ijms161226183

Kapilov-Buchman K, Portal L, Zhang Y, Fechler N, Antonietti M, Silverstein MS (2017) Hierarchically porous carbons from an emulsion-templated, urea-based deep eutectic. J Maters Chem A 5(31):16376–16385. https://doi.org/10.1039/c7ta01958k

Kiuchi H, Kondo T, Sakurai M, Guo D, Nakamura J, Niwa H, Miyawaki J, Kawai M, Oshima M, Harada Y (2016) Characterization of nitrogen species incorporated into graphite using low energy nitrogen ion sputtering. Phys Chem Chem Phys 18(1):458–465. https://doi.org/10.1039/C5CP02305J

Klapiszewski Ł, Szalaty TJ, Kurc B, Stanisz M, Skrzypczak A, Jesionowski T (2017) Functional hybrid materials based on manganese dioxide and lignin activated by ionic liquids and their application in the production of lithium ion batteries. Int J Mol Sci 18(1509):2–29. https://doi.org/10.3390/ijms18071509

Kołodyńska D, Krukowska JA, Thomas P (2017) Comparison of sorption and desorption studies of heavy metal ions from biochar and commercial active carbon. Chem Eng J 307:353–363. https://doi.org/10.1016/j.cej.2016.08.088

Kumar M, Chung JS, Hur SH (2019) Graphene composites for lead ions removal from aqueous solutions. Appl Sci 9(14):2925

Kumari P, Kaur S, Kashyap HK (2018) Influence of hydration on the structure of reline deep eutectic solvent: a molecular dynamics study. ACS Omega 3:15246–15255. https://doi.org/10.1021/acsomega.8b02447

Kyzas GZ, Mitropoulos AC (2018) Zero-cost agricultural wastes as sources for activated carbons synthesis: lead ions removal from wastewaters. Proceedings 2(652):13–21. https://doi.org/10.3390/proceedings2110652

Lawal IA, Dolla TH, Pruessner K, Ndungu P (2019) Synthesis and characterization of deep eutectic solvent functionalized CNT/$ZnCo_2O_4$ nanostructure: kinetics, isotherm and regenerative studies on Eosin Y adsorption. J Environ Chem Eng 7(1):102877. https://doi.org/10.1016/j.jece.2018.102877

Li L, Yao X, Li H, Liu Z, Ma W, Liang X (2014) Thermal stability of oxygen-containing functional groups on activated carbon surfaces in a thermal oxidative environment. J Chem Eng Japan 47(1):21–27. https://doi.org/10.1252/jcej.13we193

Li Y, Zhang X, Yang R, Li G, Hu C (2015) The role of H_3PO_4 in the preparation of activated carbon from NaOH-treated rice husk residue. RSC Adv 5(41):32626–32636. https://doi.org/10.1039/C5RA04634C

Li Y, Liu J, Yuan Q, Tang H, Yu F, Lv X (2016) A green adsorbent derived from banana peel for highly effective removal of heavy metal ions from water. Rsc Adv 6(51):45041–45048. https://doi.org/10.1039/C6RA07460J

Liu L, Fan S, Li Y (2018a) Removal behavior of methylene blue from aqueous solution by tea waste: kinetics, isotherms and mechanism. Int J Environ Res Public Health 15(7):1321. https://doi.org/10.3390/ijerph15071321

Liu S, Zhang W, Tan X, Zhao F, Huang W, Du H, Goodman BA, Lei F, Diao K (2018b) Performance of a zeolite modified with N, N-dimethyl dehydroabietylamine oxide (DAAO) for adsorption of humic acid assessed in batch and fixed bed columns. RSC Adv 8(16):9006–9016. https://doi.org/10.1039/C8RA00166A

Liu S, Duan Z, He C, Xu X, Li T, Li Y, Li X, Wang Y, Xu L (2018c) Rapid removal of Pb^{2+} from aqueous solution by phosphate-modified baker's yeast. RSC Adv 8(15):8026–8038. https://doi.org/10.1039/c7ra13545a

Liu X, Guan J, Lai G, Xu Q, Bai X, Wang Z, Cui S (2020) Stimuli-responsive adsorption behavior toward heavy metal ions based on comb polymer functionalized magnetic nanoparticles. J Cleaner Prod 253:119915. https://doi.org/10.1016/j.jclepro.2019.119915

Mi B, Wang J, Xiang H, Liang F, Yang J, Feng Z, Zhang T, Hu W, Liu X, Liu Z, Fei B (2019) Nitrogen self-doped activated carbons derived from bamboo shoots as adsorbent for methylene blue adsorption. Molecules 24(16):3012

Mouni L, Merabet D, Bouzaza A, Belkhiri L (2011) Adsorption of Pb (II) from aqueous solutions using activated carbon developed from Apricot stone. Desalination 276(1–3):148–153. https://doi.org/10.1016/j.desal.2011.03.038

Nowicki P, Kazmierczak-Razna J, Skibiszewska P, Wiśniewska M, Nosal-Wiercińska A, Pietrzak R (2016) Production of activated carbons from biodegradable waste materials as an alternative way of their utilisation. Adsorption 22(4–6):489–502. https://doi.org/10.1007/s10450-015-9719-z

Özsin G, Kılıç M, Apaydın-Varol E, Pütün AE (2019) Chemically activated carbon production from agricultural waste of chickpea and its application for heavy metal adsorption: equilibrium, kinetic, and thermodynamic studies. Appl Water Sci 9(3):56

Palomo J, Rodríguez-Mirasol J, Cordero T (2019) Methanol dehydration to dimethyl ether on Zr-loaded P-containing mesoporous activated carbon catalysts. Materials 12(13):2204

Park JH, Ok YS, Kim SH, Cho JS, Heo JS, Delaune RD, Seo DC (2016) Competitive adsorption of heavy metals onto sesame straw biochar in aqueous solutions. Chemosphere 142:77–83. https://doi.org/10.1016/j.chemosphere.2015.05.093

Patiño J, Gutiérrez MC, Carriazo D, Ania CO, Parra JB, Ferrer ML, Del Monte F (2012) Deep eutectic assisted synthesis of carbon adsorbents highly suitable for low-pressure Separation of CO_2-CH_4 Gas Mixtures. Energy Environ Sci 5(9):8699–8707

Pei Y, Xu G, Wu X, Tang K, Wang G (2019) Removing Pb (II) Ions from aqueous solution by a promising absorbent of tannin-immobilized cellulose microspheres. Polymers 11(3):548. https://doi.org/10.3390/polym11030548

Penugonda S, Mare S, Lutz P, Banks WA, Ercal N (2006) Potentiation of lead-induced cell death in PC12 cells by glutamate: protection by N-acetylcysteine amide (NACA), a novel thiol antioxidant. Toxicol Appl Pharm 216(2):197–205. https://doi.org/10.1016/j.taap.2006.05.002

Sharaf El-Deen GE, Sharaf El-Deen SEA (2016) Kinetic and isotherm studies for adsorption of Pb (II) from aqueous solution onto coconut shell activated carbon. Desalin Water Treat 57(59):28910–28931. https://doi.org/10.1080/19443994.2016.1193825

Sitko R, Turek E, Zawisza B, Malicka E, Talik E, Heimann J, Gagor A, Feist B, Wrzalik R (2013) Adsorption of divalent metal ions from aqueous solutions using graphene oxide. Dalton Trans 42(16):5682–5689. https://doi.org/10.1039/c3dt33097d

Sivachidambaram M, Vijaya JJ, Kennedy LJ, Jothiramalingam R, Al-Lohedan HA, Munusamy MA, Elanthamilan E, Merlin JP (2017) Preparation and characterization of activated carbon derived from the Borassus flabellifer flower as an electrode material for supercapacitor applications. New J Chem 41(10):3939–3949. https://doi.org/10.1039/C6NJ03867K

Su CI, Wang CL (2007) Optimum manufacturing conditions of activated carbon fiber absorbents II Effect of carbonization and activation conditions. Fibers Polym. 8(5):482–486

Tang W, Row KH (2019) Fabrication of water-compatible molecularly imprinted resin in a hydrophilic deep eutectic solvent for the determination and purification of quinolones in wastewaters. Polymers 11(5):871. https://doi.org/10.3390/polym11050871

Tang C, Shu Y, Zhang R, Li X, Song J, Li B, Zhang Y, Ou D (2017) Comparison of the removal and adsorption mechanisms of cadmium and lead from aqueous solution by activated carbons prepared from Typha angustifolia and Salix matsudana. RSC Adv 7(26):16092–16103. https://doi.org/10.1039/C6RA28035H

Usman AR, Sallam AS, Al-Omran A, El-Naggar AH, Alenazi KK, Nadeem M, Al-Wabel MI (2013) Chemically modified biochar produced from conocarpus wastes: an efficient sorbent for Fe (II) removal from acidic aqueous solutions. Adsorpt Sci Technol 31(7):625–640. https://doi.org/10.1260/0263-6174.31.7.625

Wang CP, Wu JZ, Sun HW, Wang T, Liu HB, Chang Y (2011a) Adsorption of Pb (II) ion from aqueous solutions by tourmaline as a novel adsorbent. Ind Eng Chem Res 50(14):8515–8523

Wang XS, Miao HH, He W, Shen HL (2011b) Competitive adsorption of Pb (II), Cu (II), and Cd (II) ions on wheat-residue derived black carbon. J Chem Eng Data 56(3):444–449. https://doi.org/10.1002/bkcs.11074

Wang X, Li G, Row KH (2017) Graphene and graphene oxide modified by deep eutectic solvents and ionic liquids supported on silica as adsorbents for solid-phase extraction. Bull Korean Chem Soc 38(2):251–257

Wani A, Ara A, Usmani JA (2015) Lead toxicity: a review. Interdiscip Toxicol 8(2):55–64. https://doi.org/10.1515/intox-2015-0009

Xie R, Jiang W, Wang L, Peng J, Chen Y (2013) Effect of pyrolusite loading on sewage sludge-based activated carbon in Cu(II),

Pb(II), and Cd(II) adsorption. Environ Prog Sustain Energy 32(4):1066–1073

Yadav A, Pandey S (2014) Densities and viscosities of (choline chloride+ urea) deep eutectic solvent and its aqueous mixtures in the temperature range 293.15 K to 363.15 K. J Chem Eng Data 59(7):2221–2229

Yang G, Hu H, Zhou Y, Hu Y, Huang H, Nie F, Shi W (2012) Synthesis of one-molecule-thick single-crystalline nanosheets of energetic material for high-sensitive force sensor. Sci Rep 2(1):1–7. https://doi.org/10.1038/srep00698

Yantasee W, Lin Y, Fryxell GE, Alford KL, Busche BJ, Johnson CD (2004) Selective removal of copper (II) from aqueous solutions using fine-grained activated carbon functionalized with amine. Ind Eng Chem Res 43(11):2759–2764

Yao X, Xu K, Liang Y (2016) Comparing the thermo-physical properties of rice husk and rice straw as feedstock for thermochemical conversion and characterization of their waste ashes from combustion. BioResources 11(4):10549–10564

Yin J, Deng C, Yu Z, Wang X, Xu G (2018) Effective removal of lead ions from aqueous solution using nano illite/smectite clay: isotherm, kinetic, and thermodynamic modeling of adsorption. Water 10(2):1–13. https://doi.org/10.3390/w10020210

Zhang J, Li L, Li Y, Yang C (2016) Microwave-assisted synthesis of hierarchical mesoporous nano-TiO_2 / cellulose composites for rapid adsorption of Pb^{2+}. Chem Eng J. https://doi.org/10.1016/j.cej.2016.11.007

Zhao Y, Mao Q, Liu Y, Zhang Y, Zhang T, Jiang Z (2014) Investigation of cytotoxicity of phosphoryl choline modified single-walled carbon nanotubes under a live cell station. Biomed Res Int 2014:1–12. https://doi.org/10.1155/2014/537091